Pourbaix diagram of astatine revisited: experimental investigations

Lu Liu, Rémi Maurice, Nicolas Galland, Philippe Moisy, Julie Champion, Gilles F Montavon

Pourbaix diagram of astatine revisited: Experimental investigations

Lu Liu[a†], Rémi Maurice[a, b], Nicolas Galland[c], Philippe Moisy[d], Julie Champion[a] and Gilles Montavon[a]*

a. IMT Atlantique, Nantes Université, CNRS, SUBATECH, F-44000 Nantes, France

b. Univ Rennes, CNRS, ISCR (Institut des Sciences Chimiques de Rennes) — UMR 6226, 35000 Rennes, France

c. Nantes Université, CNRS, CEISAM UMR 6230, F-44000 Nantes, France

d. CEA, DES, ISEC, DMRC, Univ Montpellier, Marcoule, France.

KEYWORDS

Astatine, speciation, standard redox potential, Pourbaix diagram

ABSTRACT

The Pourbaix diagram of an element displays its stable chemical forms with respect to the redox potential and pH of the solution, whose knowledge is fundamental for understanding and for anticipating the chemistry of the element in a specified solution. Unlike most halogens, the

Pourbaix diagram in aqueous phase for astatine (At, Z = 85) is still under construction. In particular, the domains of predominance of two astatine species assumed to exist in alkaline conditions, At^- and $AtO(OH)_2^-$, need to be refined. Through high-performance ion-exchange chromatography, electromobility measurements and competition experiments, the existence of At^- and $AtO(OH)_2^-$ has been confirmed and the associated standard potential has been determined for the first time, being 0.86 ± 0.05 V *vs.* SHE. Based on these results, a revised version of astatine's Pourbaix diagram is proposed, covering the three oxidation states of astatine existing in the thermodynamically stability range of water: At(–I), At(I) and At(III) (as At^-, At^+, AtO^+, AtO(OH) and $AtO(OH)_2^-$).

Introduction

The Pourbaix diagram, also known as the potential–pH diagram, is a thermodynamic chart displaying the possible stable species of an element with respect to both the pH and the redox potential (Eh), usually in aqueous and non-complexing solution. Each contour of this diagram materializes an equilibrium, *i.e.* the conditions where the activities for the predominant soluble species on each side of it are equal.[1] Pourbaix diagrams are not only of fundamental interest, but also have been proved to be very useful in various applied fields, such as corrosion studies, geoscience, and environmental research.[2–4] Even though such diagrams have been well established for numerous elements, information is limited for some (rare) ones, notably the element 85, astatine (At). Indeed, astatine is a radioelement, and all of its isotopes are short-lived ($t_{1/2} \leq 8.1$ h). Only minute quantities can be produced artificially, leading to astatine solutions at ultra-trace concentrations (typically below 10^{-10} mol·L^{-1}). Conventional spectroscopic tools are therefore barely applicable to identify astatine species. Even more than 80 years after the discovery of astatine,[5] its chemical properties remain not well-established. Beyond the scientific interest, the

need to better understand the chemistry of astatine is motivated by the potential use of the ^{211}At radioisotope in targeted alpha-particle therapy (TAT). There is a growing attention for the emerging field of TAT drugs following the success and FDA approval of Xofigo®, an alpha-emitting based radiopharmaceuticals.[6] The catalog of alpha-emitters available for use as drugs needs to be expanded. ^{211}At is one of the most promising candidates due to its suitable physical properties ($t_{1/2}$ = 7.2 h and 100% alpha-emitter), and several clinical trials have been led.[7,8] However, TAT requires ^{211}At to be attached to a biological vector and the knowledge of astatine speciation in solution is essential for the development of radiolabeling approaches.[9,10]

The reported investigations of the chemical forms of astatine remain based on limited technical approaches. Some knowledge was acquired on astatine species according to (i) their behaviors in coprecipitation experiments, electromobility measurements, thin-layer chromatography measurements and competition experiments in a biphasic system, and (ii) comparisons with iodine chemistry.[11,12] These sketchy analyses are insufficient to figure out the exact nature of the species involved in many reactions, with sometimes inconsistencies in the literature.[10,13] A more detailed analysis of the data, however, allows tracing back important information such as the charge,[14,15] the stoichiometry of the species[16,17] and quantitative data describing the formation of the species.[18–20] Molecular modeling has also been proved to be of great help since it can provide extra information at the molecular level and quantitative data that can be compared with experimental values.[21–24] The nature of the studied species can be assessed through such comparison.

Combining experimental and computational approaches, five astatine species in the thermodynamically stability zone of water were characterized and a Pourbaix diagram of astatine can be drawn, as shown in Figure 1.[15,18,19,25] In this diagram, At^- is present in reducing conditions over the whole pH range. In acidic solutions with the increasing redox potential, two cationic

species were proposed, At^+ and AtO^+, with oxidation states of +1 and +3, respectively. Under oxidizing conditions with the increasing pH, two hydrolyzed species predominate, AtO(OH) and $AtO(OH)_2^-$. The conversions among these species have also been investigated, which forms the solid lines in the diagram, with the parameters listed in Table S1. However, there are still some equilibria that have not been examined as shown by dashed lines in Figure 1.

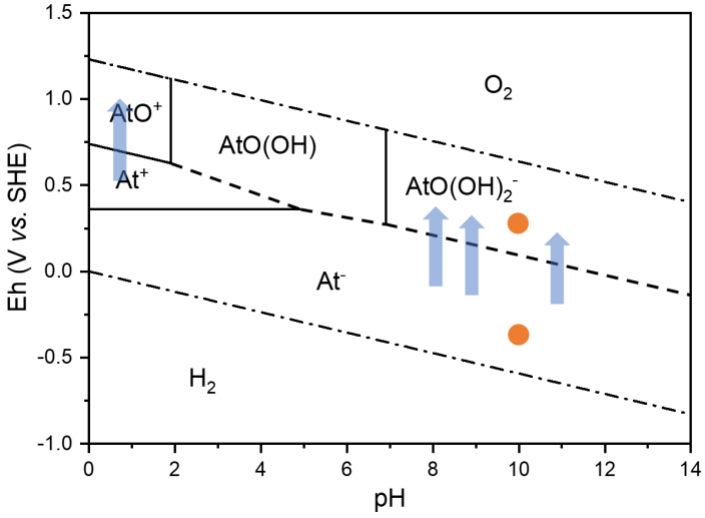

Figure 1. Pourbaix diagram of astatine derived from selected published data.[14,15,18,19,25] Dashed lines correspond to indirectly determined equilibria. The orange points figure the experimental conditions used for the high-performance ion-exchange chromatography or electromobility measurements, and the blue arrows represent the experimental conditions for the competition experiments. The region between these two dash-dotted lines is the window of stability of H_2O.

The reaction between At^- and $AtO(OH)_2^-$ in alkaline conditions has to be experimentally characterized to go beyond the previous indirect characterization (based on the combination of parameters corresponding to other equilibria).[18,19,25] In addition, if the reaction $At^-/AtO(OH)_2^-$ is confirmed by new data, it would validate the Pourbaix diagram with dashed equilibria presented

in Figure 1. Otherwise the actual Pourbaix diagram should be revised and possibly account for the existence of other At species.

This work is focused on the speciation of astatine in alkaline conditions and on quantifying the reaction between the relevant species, according to the strategy displayed in Figure 1. Firstly, astatine species in reducing and non-reductive conditions at pH = 10 (orange points) are characterized by high-performance ion-exchange chromatography (HPIEC) and electromobility measurements. The astatine species present in alkaline and reducing conditions is (are) denoted At_{red}, while that in alkaline and non-reductive conditions is (are) denoted At_{ox}. The aims are to identify how many species exist in each domain and to determine their charge. Secondly, the change in astatine speciation is tracked by liquid/liquid competition experiments with increasing redox potential at fixed pH. The standard potential of this reaction is then derived. Finally, all the results are discussed and compared with literature data, leading to a revised Pourbaix diagram in aqueous solution.

Results

Characterization of astatine species in alkaline conditions

The first step was to identify the number of species to be considered in reducing and non-reductive conditions. In both cases, only one peak is found in the HPIEC radiochromatogram and the electromobility radiochromatogram (Figure 2). Note that the peak at the position of injection is considered as ^{211}At and/or ^{123}I trapped in the injection outlet instead of a neutral species, because its position does not change over time (Figure S1), which is supposed to happen for a neutral species due to the Electroosmosis effect.[15] Considering that these two techniques are based on different separation mechanisms, the chemical affinity of ions for the resin in HPIEC and the

charge/size ratio of ions in electromobility measurements, there can be only one species existing for each condition, reducing or non-reductive (it is unlikely that two coexisting species of astatine have the same values for such different properties).

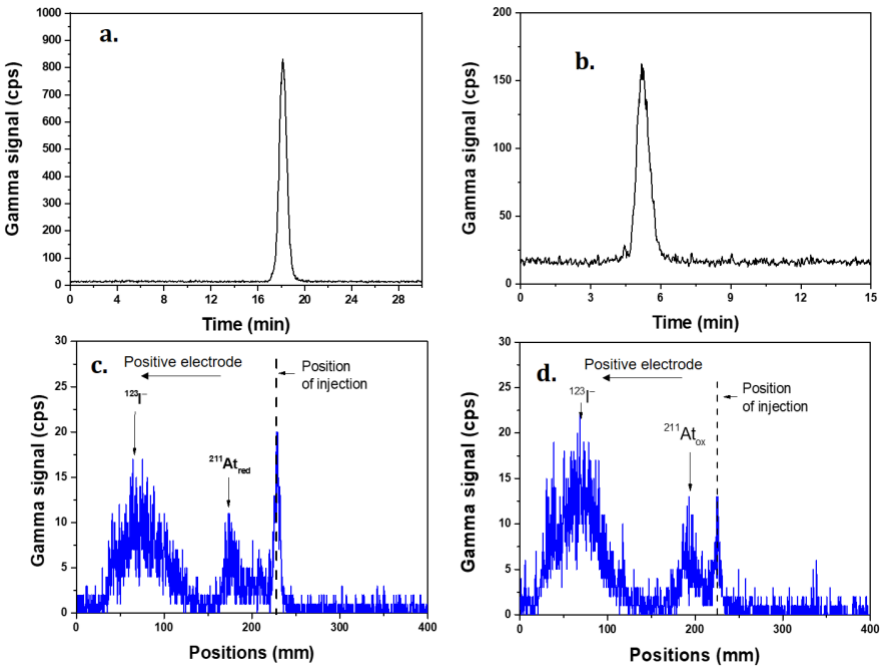

Figure 2. a) HPIEC radiochromatogram of At_{red}. Flow rate: 350 µL·min^{-1}; eluent: 0.085 M NaCl/10^{-4} M NaOH/10^{-4} M DTT; At sample prepared in 10^{-4} M NaOH/10^{-4} M DTT. b) HPIEC radiochromatogram of At_{ox}. Flow rate: 350 µL·min^{-1}; eluent: 0.05 M $NaClO_4$/10^{-4} M NaOH; At samples prepared in 0.05 M $NaClO_4$/10^{-4} M NaOH. c) Electromobility radiochromatogram of $^{123}I^-$ and $^{211}At_{red}$. Electrolytes and samples prepared in 10^{-4} M NaOH/10^{-4} M DDT/0.1 M NaCl. d) Electromobility radiochromatogram of $^{123}I^-$ and $^{211}At_{red}$. Electrolytes and samples prepared in 10^{-4} M NaOH/0.1 M $NaClO_4$.

The second step was to investigate the nature of At_{red} and At_{ox}. Figure 3 presents HPIEC results which show the influence of the ionic strength in the eluent (NaCl concentration) on the retention

factor of Br^-, I^-, $S_2O_3^{2-}$ and At_{red}. The log-log representation of the retention factor as a function of the ionic strength is linear, as expected for an ionic column and ionic species.[26] The slope for the astatine species is close to that for I^- and Br^-, while it is almost half of the slope for $S_2O_3^{2-}$. These results testify obviously of a –1 charge for At_{red}.

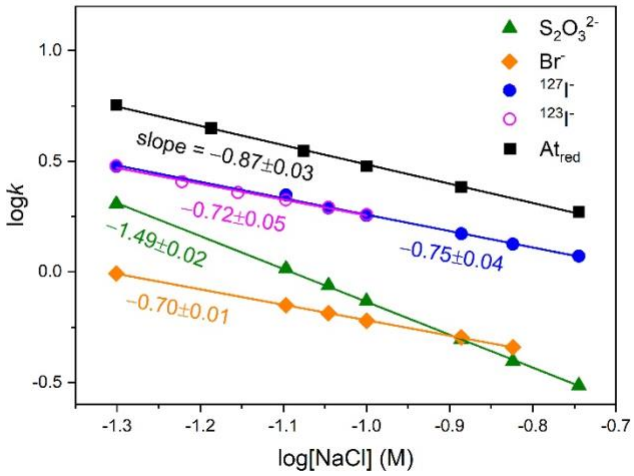

Figure 3. HPIEC results for At_{red} (squares), I^- (circles), and Br^- (diamond) and $S_2O_3^{2-}$ (triangles) under alkaline and reducing conditions: plot of the retention factor *k* as a function of NaCl molarity in the NaCl/10^{-4}M NaOH/10^{-4}M DTT eluent (flow rate: 350 mL·min^{-1}). The solid lines are linear fittings of the results and the slopes are indicated below the curves.

The electromobility measurements provide even more information. Firstly, the peak representing At species moved toward the positive electrode during the experiments (Figure 2c, d), evidencing the anionic nature of At_{red} and At_{ox}. Secondly, the apparent mobility of the different ^{211}At species in comparison to $^{123}I^-$ is determined by introducing these species in the electromobility device following the method described by *Guo et al.*[15] Under the applied (pH, Eh) conditions, iodide is the predominant species according to the Pourbaix diagram of iodine.[27] From the radiochromatogram of ^{211}At and ^{123}I, the positions of At_{red}, At_{ox} and iodide in the migration tube

at different moments can be identified, thus apparent mobilities (μ_{app}) can be obtained. More details related to the calculations can be found in the Supporting Information (Figure S1 and Table S2). Table 1 lists the relative apparent mobility of astatine species with respect to I^-. The difference in mobility between At_{ox} and I^- is significantly more important than that between At_{red} and I^-, which implies At_{red} and At_{ox} are different species. Moreover, some of us have experimentally shown that the mobility of At^- is close to that of I^-,[15] which was also supported by molecular dynamics simulations.[28] As a reminder, the previous experiments were conducted in an acidic environment. Hence the present results in alkaline conditions are found in good agreement.

Table 1. Difference in the apparent mobility of some astatine species compared to I^- species.

Species	μ_{app} ($^{211}At - {}^{123}I^-$) (10^{-4} $cm^2.V^{-1}.s^{-1}$)	Ref.
At_{ox}	3.3 ± 1.0	this work
At_{red}	0.1 ± 0.2	this work
At^-	0.29 ± 0.79	[15]

In short, it was demonstrated that At_{red} holds a –1 charge and has a mobility close to that of At^-. It is therefore reasonable to consider that At_{red} is At^-. So astatide (At^-) exists under reducing conditions in both acidic and alkaline media. This is consistent with the series of halogens: anionic X^- exists in reducing conditions over the whole pH range. As for At_{ox}, the HPIEC and electromobility measurements evidenced as well a negative species, but it is different from At_{red}.

Identification of At_{ox}

After identifying At_{red} as the At^- species, liquid/liquid competition experiments have been carried out for studying the passage At^-/At_{ox} and characterizing At_{ox}. The pH of the solution was set between 8 and 11 while the potential increased from –0.20 V up to 0.35V *vs.* SHE (Figure 4 and Figure S2). Under small potential values, the distribution ratio of astatine (*D*) keeps constant and close to 0, *i.e.* At^- is not extracted into the organic phase. Then *D* increase sharply at a threshold of potential, indicating a change of astatine speciation: At^- becomes At_{ox}, and the latter is more soluble in the organic phase. Moreover, the Eh of inflection point depends on pH, which implies that the speciation change involves the exchange of protons, in addition to the exchange of electrons. Then the quantitative analysis of the experimental data, taking into account the various equilibria occurring under the experimental conditions, makes it possible to uncover the chemical form of At_{ox} and obtain the quantitative parameters allowing describing its formation.

In reducing conditions, *D* is ruled by the distribution of At^- between the two phases according to Equation (1). Within the studied potential range, *D* keeps increasing. However, the other plateau of *D* governed by the distribution of At_{ox} (Equation (2)) was not observed due to the limitation of the used oxidizing agents. In these two equations, D_1 and D_2 are the distribution ratio of At^- and At_{ox} between the biphasic aqueous/DIPE system, respectively, and the overlined species are in the organic phase.

$$\mathrm{At}^- \overset{D_1}{\Leftrightarrow} \overline{\mathrm{At}^-} \quad (1)$$

$$\mathrm{At}_{ox} \overset{D_2}{\Leftrightarrow} \overline{\mathrm{At}_{ox}} \quad (2)$$

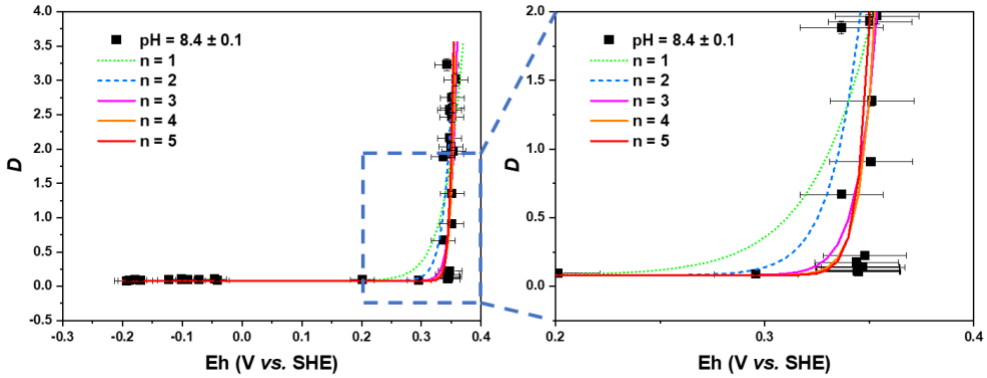

Figure 4. Distribution ratio of At in biphasic aqueous/DIPE system (pH = 8.4 ± 0.1) as function of potential of the sample (black square symbols). The colored lines show the simulations of *D* supposing an exchange of *n* electrons from At^- to form At_{ox}.

Suppose that the formation of At_{ox} from At^- involves an exchange of *n* electrons and *m* protons and a production of *k* water molecules:

$$At_{ox} + ne^- + mH^+ \Leftrightarrow At^- + kH_2O \quad (3)$$

where $n \geq 1$ (because a speciation change is evidenced), $m \geq n$ (because At_{ox} holds a negative charge) and $k \geq 0$.

According to the Nernst equation, the relationship between the potential of the solution (*E*) and the concentrations of At^- and At_{ox} can be written as Equation (4):

$$E = E^{0\prime} + \frac{0.06}{n} \log \frac{\gamma_{At_{ox}}[At_{ox}]}{\gamma_{At^-}[At^-]} \quad (4)$$

with γ_{At^-} and $\gamma_{At_{ox}}$ being the activity coefficient of At^- and At_{ox}, and

$$E^{0\prime} = E^0 - 0.06 \frac{m}{n} pH \quad (5)$$

In Equation (5), E^0 is the standard potential of At_{ox}/At^- redox couple and $E^{0\prime}$ is the apparent potential of At_{ox}/At^- at a fixed pH. Note that $\frac{\gamma_{At_{ox}}}{\gamma_{At^-}} = 1$ if At_{ox} is of –1 charge, or < 1 if the charge of At_{ox} is < –1. Here we firstly consider the case that $\frac{\gamma_{At_{ox}}}{\gamma_{At^-}} = 1$, and discuss later other possibilities.

D of astatine, experimentally calculated as the ratio of specific activity of astatine in the organic phase to the aqueous phase, can be written as the following equation:

$$D = \frac{[\overline{At_{ox}}] + [\overline{At^-}]}{[At_{ox}] + [At^-]} = \frac{D_2 + D_1 \frac{[At^-]}{[At_{ox}]}}{1 + \frac{[At^-]}{[At_{ox}]}} \quad (6)$$

Combining Equation (4) and (6), *D* can be expressed as following:

$$D = \frac{D_2 + D_1\, 10^{\frac{-n\,(E - E^{0\prime})}{0.06}}}{1 + 10^{\frac{-n\,(E - E^{0\prime})}{0.06}}} \quad (7)$$

The experimental data were then fitted with D_1, *n* and $E^{0\prime}$ as adjustable parameters. Note that D_2 cannot be fully determined, and it was at first fixed to be 15, the maximum value reached in this work. The only information obtained from experimental data is that D_2 should be greater than 15. Among the unknown parameters, *n* should be a natural number and Figure 4 shows the fitting results according to the value of *n*. With *n* = 1 and *n* = 2, it is obvious that the sharp increase of *D* cannot be explained. For $n \geq 3$, the fitting curves are very close and all can fairly explain the experimental data. Regardless of the value of *n* (≥ 3), the obtained $E^{0\prime}$ value from the fitting keeps unchanged, given the uncertainties. Therefore, a set of (pH, $E^{0\prime}$) value was obtained as shown in Figure 5.

According to Equation (5), it is found that $m/n = 0.81 \pm 0.24$ and, since $m \geq n$ (*cf.* above), we can reasonably conclude that $m = n$.

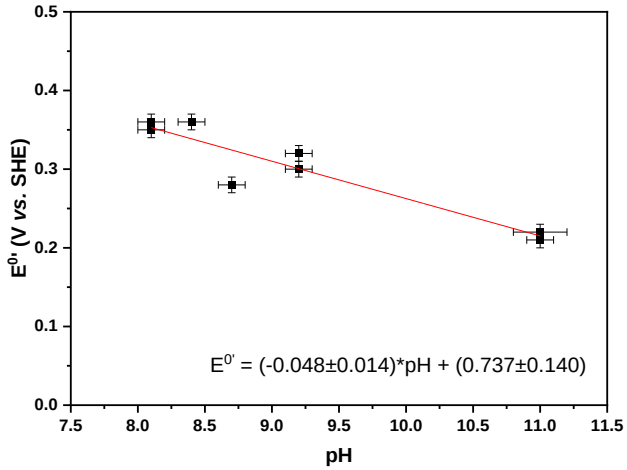

Figure 5. Relationship between pH and $E^{0'}$ obtained from the data analysis of the competition experiments.

For the preset $\frac{\gamma_{At_{ox}}}{\gamma_{At^-}}$ value, the tests of fitting show that this parameter does not have an observable impact on the shape of curves; the conclusion for $n \geq 3$ is therefore maintained. However, the change of $\frac{\gamma_{At_{ox}}}{\gamma_{At^-}}$ value will shift the obtained $E^{0\prime}$ value. With $\frac{\gamma_{At_{ox}}}{\gamma_{At^-}} = 0.01$ (approximately for At_{ox} holds –4 charge in the experimental conditions), the fitting of the obtained (pH, $E^{0\prime}$) sets gives a very similar slope for the case that $\frac{\gamma_{At_{ox}}}{\gamma_{At^-}} = 1$. Consequently, the conclusion that m = n is also maintained.

If $n = m = 3$, the oxidation state of At_{ox} is +2. It is unlikely since this oxidation state has never been reported in the literature for astatine or any other halogen.

If $n = m = 4$, the oxidation state of At_{ox} is +3. Three chemical forms for At_{ox} are possible: $At(OH)_4^-$, AtO_2^- and $AtO(OH)_2^-$. $At(OH)_4^-$ would be a hydrolyzed species of At^{3+}, but the latter is inconsistent with the At(III) species proved to exist in acidic conditions, AtO^+.[18] The AtO_2^- form would result from deprotonation of the AtO(OH) species,[25] but it can also be ruled out. According

to quantum mechanical calculations it would exist only for pH > 11,[25] conditions that are not compatible with current experiments. $AtO(OH)_2^-$ as the second hydrolyzed form of the AtO^+ species is therefore the most likely species. In the conditions where At_{ox} is obtained, $AtO(OH)_2^-$ allows a satisfactory description of the experimental data.[25] Its conversion from At^- involves therefore an exchange of 4 electrons and 4 protons. Larger *n* values would result in a more unfavorable reaction kinetics due to exchange of a larger amount of protons/electrons, while the experimental results can already be confronted with $n = m = 4$.

Determination of the standard potential $E^0_{AtO(OH)_2^-/At^-}$

Considering that At_{ox} is $AtO(OH)_2^-$, the standard potential $E^0_{AtO(OH)_2^-/At^-}$ can be deduced from the liquid/liquid competition experiments according to the Nernst equation (4–5) for the reaction (8):

$$AtO(OH)_2^- + 4e^- + 4H^+ \rightleftharpoons At^- + 3H_2O \quad (8)$$

The determined values for the different pH conditions are listed in Table 2, with an average value: $E^0_{AtO(OH)_2^-/At^-} = 0.86 \pm 0.05 V\ vs.\ SHE$.

Table 2. Redox potential related to the speciation change at different pH.

pH	$E^{0\prime}_{AtO(OH)_2^-/At^-}$ (V *vs.* SHE)	$E^0_{AtO(OH)_2^-/At^-}$ (V *vs.* SHE)
8.1 ± 0.1	0.36 ± 0.02	0.85 ± 0.02
8.1 ± 0.1	0.35 ± 0.02	0.84 ± 0.02
8.4 ± 0.1	0.36 ± 0.02	0.86 ± 0.02
8.7 ± 0.1	0.28 ± 0.02	0.80 ± 0.02
9.2 ± 0.1	0.32 ± 0.02	0.87 ± 0.02

9.2 ± 0.1	0.32 ± 0.02	0.87 ± 0.02
11.0 ± 0.1	0.21 ± 0.02	0.87 ± 0.02
11.0 ± 0.2	0.22 ± 0.02	0.88 ± 0.02
Average		0.86 ± 0.05

Applying $E^0_{\mathrm{AtO(OH)_2^-/At^-}} = 0.86$ V *vs.* SHE, together with the literature data, $E^0_{\mathrm{At^+/At^-}} = 0.36$ V *vs.* SHE,[18] $\log K_{\mathrm{AtO^+,hyd,1}} = -1.9$,[19] and $\log K_{\mathrm{AtO(OH),hyd,2}} = -6.9$,[25] a new version of the Pourbaix diagram of astatine can be built. It is shown in Figure 6 and the related characteristic values are presented in Table 3. The experimental results (Table S3) obtained by different authors[13,18,29] for redox couples in acidic conditions at 25 °C are also presented in this figure.

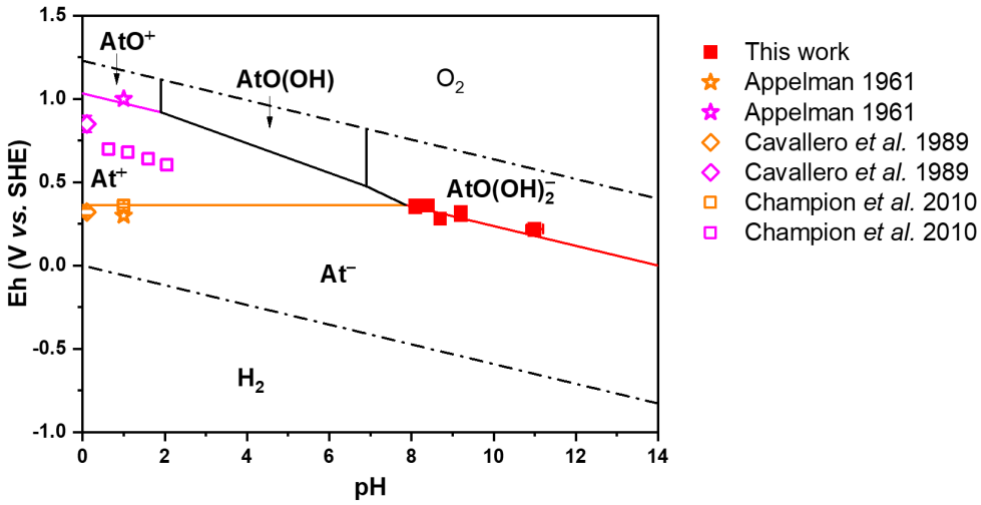

Figure 6. Pourbaix diagram of astatine (25°C) constructed by considering $E^0_{\mathrm{At^+/At^-}} = 0.36$ V *vs.* SHE, $E^0_{\mathrm{AtO(OH)_2^-/At^-}} = 0.86$ V *vs.* SHE, $\log K_{\mathrm{AtO^+,hyd,1}} = -1.9$ and $\log K_{\mathrm{AtO(OH),hyd,2}} = -6.9$. The points in the diagram are experimental results.[13,18,19,25,29] The colors of symbols are in agreement with the considered equilibria. The region between these two dash-dotted lines is the window of stability of H_2O.

Table 3. Parameters used for the construction of the Pourbaix diagram presented in Figure 6.

Species	Parameter	Value	Ref.
$AtO^+/AtO(OH)$	$\log K_{AtO^+,hyd,1}$	-1.9	[19]
$AtO(OH)/AtO(OH)_2^-$	$\log K_{AtO(OH),hyd,2}$	-6.9	[25]
At^+/At^-	$\log K_{At^+/At^-}$	-30.8	[18]
	$E^0_{At^+/At^-}$	0.36 V $vs.$ SHE	
AtO^+/At^+	$\log K_{AtO^+/At^+}$	-6.5	this work
	$E^0_{AtO^+/At^+}$	1.09 V $vs.$ SHE	
$AtO(OH)_2^-/At^-$	$\log K_{AtO(OH)_2^-/At^-}$	-28.5	this work
	$E^0_{AtO(OH)_2^-/At^-}$	0.86 V $vs.$ SHE	
$AtO(OH)/At^+$	$\log K_{AtO(OH)/At^+}$	-4.6	this work
	$E^0_{AtO(OH)/At^+}$	1.14 V $vs.$ SHE	
$AtO(OH)_2^-/At^+$	$\log K_{AtO(OH)_2^-/At^+}$	2.3	this work
	$E^0_{AtO(OH)_2^-/At^+}$	1.35 V $vs.$ SHE	

Discussions

Since no new species has been discovered in alkaline conditions, the speciation of astatine proposed in the water stability zone is confirmed with 3 oxidation states (–1, +1 and +3) and 3 acido-basic forms for At(III), *i.e.* At^-, At^+, AtO^+, AtO(OH) and $AtO(OH)_2^-$ are the existing predominant species. However, some domains in the Pourbaix diagram have been modified. In the revised Pourbaix diagram (Figure 6), the redox and acido-basic equilibrium of At^+/At^-,

$AtO^+/AtO(OH)$ and $AtO(OH)/AtO(OH)_2^-$ keep unchanged compared to the previous version (Figure 1). Several redox potential for the At^+/At^- couple have been proposed, which are in good agreement with each other.[13,18,29] Here was retained the value derived from the largest number of experimental data: 0.36 ± 0.01 V $vs.$ SHE .[18] Conversely, only one acido-basic constant measurement is reported for each of the $AtO^+/AtO(OH)$ and $AtO(OH)/AtO(OH)_2^-$ equilibria.[19,25]

A large discrepancy for $E^0_{AtO^+/At^+}$ exists among the reported values in the literature.[13,18,29] Using the value determined in this work for $E^0_{AtO(OH)_2^-/At^-}$, it is deduced that $E^0_{AtO^+/At^+} = 1.09$ V $vs.$ SHE (Table 3) as shown by the purple-colored line in Figure 6. This value is in good agreement with the data published by Appelman,[29] while two previously reported values, $E^0_{AtO^+/At^+} = 0.74 \pm 0.01$ V $vs.$ SHE[18] and 0.80 ± 0.05 V $vs.$ SHE,[13] are significantly below (Figure 6).

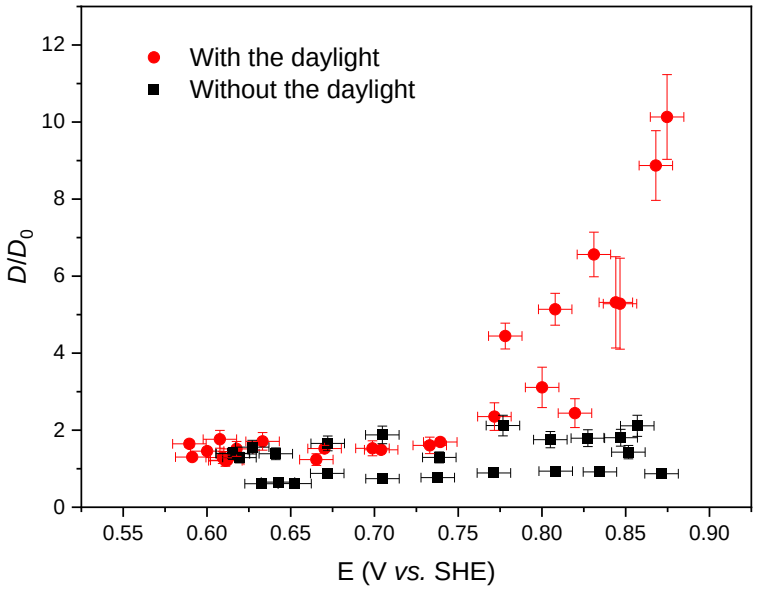

Figure 7. Distribution ratio of At in biphasic aqueous/DIPE system (pH = 1) as function of the redox potential adjusted by Fe(II)/Fe(III) redox couple. Red squares and black circles represent

experiments performed with or without the daylight, respectively. D_0 is the distribution ratio of At without the presence of iron couple.

Appelman has judiciously noticed that the redox reaction between At^+ and AtO^+ in acidic media is sensitive to the light when iron and vanadium couples are used as buffer for adjusting Eh in samples.[29] This may lead to a gross shift of the studied chemical equilibrium, resulting in an underestimation of the standard potential. The iron couple was notably used in ref. [18] for controlling the potential of solution. In order to confirm the Appelman's observation, new investigations of the evolution of astatine species has been done by liquid/liquid competition method at pH = 1 and oxidizing conditions controlled by the Fe^{2+}/Fe^{3+} couple. Two series of experiments were performed, one with Pyrex tubes covered by an aluminum foil and the other not. As shown in Figure 7, it turns out that astatine behaves differently with or without the daylight. The series with light suggests a change of astatine speciation from a potential around 0.8 V $vs.$ SHE, whereas no changes in the distribution ratio of astatine is observed for the series without light. These results agree with Appelman and might also explain an underestimated value of the redox potential in ref. [18]. As for the results of Cavallero *et al.* ($E^0_{AtO^+/At^+} = 0.80 \pm 0.05$ V $vs.$ SHE),[13] the reason of discrepancy has not been identified. Cr(VI)/Cr(III) was used to maintain the redox conditions and it is not known if this couple leads to photosensitivity for astatine species as iron and vanadium do. However, a similar work based on chromatography has led to a value of 1.09 V $vs.$ SHE (at 80 °C).[30] Though the author claimed that the value proposed was approximate, it questions the reproducibility of this method. Besides, the high nitric acid concentration (1M HNO_3) used by Cavallero *et al*., is not inert.[13] If the complexing effect of nitrate anion[31] is not very different compared to perchloride[18] anion used in this work, the redox effect produced by alpha radiolysis of HNO_3 may modify the potential. Indeed, it is reported[32] that the

alpha radiolysis of nitric acid produced nitrous acid, which may cause some shift of the redox potential of the solution due to reaction with Cr(VI)/Cr(III) buffer. Note that the determination in the present work of $E^0_{\mathrm{AtO(OH)_2^-/At^-}}$ does not rely on the use of iron, vanadium or any other metallic cation redox couple. Moreover, this very first value of $E^0_{\mathrm{AtO(OH)_2^-/At^-}}$ leads to a good agreement with reported $E^0_{\mathrm{AtO^+/At^+}}$ values from the literature. Therefore, the revised version of Pourbaix diagram shown in Figure S3 can be considered reliable.

From the Pourbaix diagram of astatine, one remarkable phenomenon that can be deduced is the disproportionation of $\mathrm{At^+}$ into $\mathrm{At^-}$ and $\mathrm{AtO(OH)_2^-}$, for pH > 8.25, according to the equation (9).

$$2\mathrm{At^+} + 3\mathrm{H_2O} \rightleftharpoons \mathrm{AtO(OH)_2^-} + \mathrm{At^-} + 4\mathrm{H^+} \quad (9)$$

Given the minute quantities of astatine, whether this reaction will happen in the reality is uncertain due to the kinetically constraint, although it is thermodynamically possible (log K = –33).

The Pourbaix diagram is as well limited to the stability region of water. According to the literature, two other oxidation states may exist in highly oxidizing conditions: +5 and +7. A sketch of a tentative Pourbaix diagram incorporating these two species is presented in Figure 8. At(V) has been reported to occur in acidic, neutral and alkaline medium with the presence of strong oxidizing agents such as $S_2O_8^{-}$ (hot solution), KIO_4 and HClO. It is hypothesized to be AtO_3^- due to similarities with the behavior of IO_3^-.[12,29,33–36] However, the quantitative analyses are very limited in the literature. An apparent potential of 1.5 V at pH = 1 for At(V)/At(III) has been proposed by Appelman,[29] consistently with the standard potential above 1.5 V reported by Cavallero.[13] At(VII) is expected in neutral or alkaline solution with the presence of KIO_4 or XeF_2, but is unstable in acidic conditions.[12,34–37] At(VII) is assumed to be AtO_4^- but no quantitative data have been reported for supporting this hypothesis. Obviously, it would be interesting to obtain more quantitative information on these species and to be able to name them.

Conclusion

Astatine speciation in alkaline conditions has mainly been studied in this work, in order to test the parameters obtained so far to describe the speciation of astatine in the stability region of water. Using HPIEC measurements, electromobility measurements, and liquid/liquid competition experiments, At^- and $AtO(OH)_2^-$ were identified to be the predominant forms in reducing and oxidizing conditions, respectively. These results validate the existence of already characterized species in the water stability zone. Moreover, the first experimental value for the standard potential of $AtO(OH)_2^-/At^-$ couple is derived in this work, being 0.86 ± 0.05 V *vs.* SHE. Based on this result and some from the literature, the standard potential for the species in acidic conditions has been revised, and finally a revised Pourbaix diagram of astatine based on updated parameters has been proposed. The predominance domains of At^- and At^+ species appears more extended. In the meanwhile, other species may exist beyond the domain of water stability, but this remains to be explored using quantitative analytical techniques.

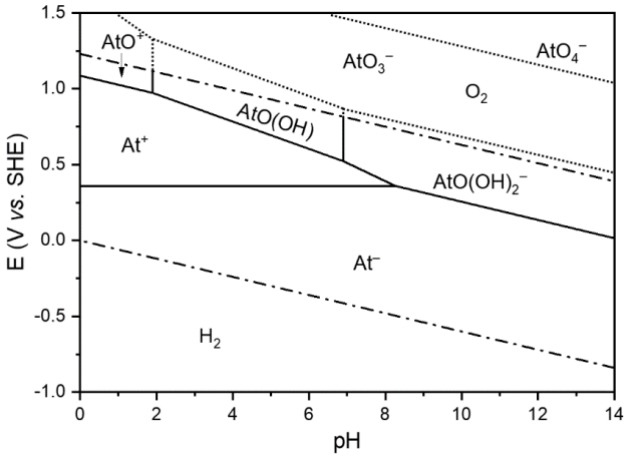

Figure 8. Sketch of Pourbaix diagram of astatine including including At(-I), At(+I), At(+III), At(V) and At(VII) species. The region between these two dash-dotted lines is the window of stability of H_2O. The dotted lines represent some astatine speciation equilibria to be determined.

Experimental section

Materials

Chemicals

All chemicals are commercially available and of analytical grade or better. The solutions were freshly prepared using Milli-Q deionized water.

Radioactive sources

^{123}I ($t_{1/2}$ = 13.2 h) was purchased from Curium (Paris, France) as sodium iodide-^{123}I (reference: I-123-S-2) with a specific activity of 18.5 MBq·mL^{-1} in an aqueous solution and with a radiochemical purity ≥ 95%.

^{211}At was produced through the $^{209}Bi(\alpha, 2n)^{211}At$ nuclear reaction at the ARRONAX cyclotron (Nantes, France). ^{209}Bi targets were irradiated by alpha external beams accelerated and downgraded to 28.6 MeV.[38] After irradiation, astatine was extracted by a dry distillation method,[39] and finally was recovered in chloroform with a specific activity close to 500 MBq·mL^{-1}. The radionuclide purity of ^{211}At was verified by γ-ray spectroscopy with high purity germanium (HPGe) detector. In the present work, the ^{211}At sources were back-extracted in the desired aqueous medium by a series of steps. Firstly, chloroform was evaporated to dryness using a nitrogen gas flux. No astatine leakage has been identified within this step.[15] Secondly, about 500 µL of the desired solution (for reducing or non-reductive conditions) was added in the vial and waited for at least two hours to retrieve At in solutions with the expected form, *i.e.* At_{red} or At_{ox}.

Methodologies and analytical tools.

The stock solutions of dithiothreitol (DTT), Piperazine-N,N′-*bis*(3-propanesulfonic Acid) (PIPPS), NaCl, $NaClO_4$, $Na_2S_2O_8$, Na_2SO_4 were prepared by dissolving the corresponding salts. The stock solution of NaOH was prepared from a concentrated volumetric NaOH solution. All preparations were performed under inert gas (argon or nitrogen) conditions, as well as the measurements by competition experiments. While such a precaution was not possible for those obtained by HPIEC and electromobility. Note that the used HPIEC device includes a degasser for the eluent. As for electromobility, a pre-test was performed without radioactive source. It showed that after the exposure of three hours (maximum time for a measurement) of the electrolyte in the equipment, there is no distinct change in the pH and in the potential. It is therefore assumed that dissolved carbonates do not significantly affect the speciation of At(I) and At(III) species under our conditions.

Irrespective of the method used, the pH and the potential of the solutions were systematically measured at equilibrium. An electrode (Inlab) freshly calibrated with standard pH buffers (pH 7.00 and 10.00, Merck) and a Pt combined redox electrode (Metrohm) calibrated with a redox buffer ($Fe(SCN)_6^{3-}/Fe(SCN)_6^{4-}$, 220 mV/Pt/SCE, Radiometer Analytical) were used to measure the pH and the potential (E, V *vs.* SHE) of the aqueous phase at equilibrium, respectively. The potential effect of oxidizing and reducing agents used in this work (DTT, $S_2O_8^{2-}$ and SO_4^{2-}) on astatine speciation were investigated beforehand, and more details can be found in the Supporting Information (Figure S4 and S5).

HPIEC experiments.

In an HPIEC-based experiment, different ions are separated according to their different chemical affinity towards an ionic-exchange column and characterized by the time retained in the column, *i.e.* the retention time (t_r). Here, At_{red} and At_{ox} were prepared using the reducing (10^{-4} M NaOH/10^{-4} M DTT; pH = 10.0 ± 0.2, E = –0.15 ± 0.02 V *vs.* Standard Hydrogen Electrode (SHE)) and the oxidizing (10^{-4} M NaOH/0.05 M $NaClO_4$; pH = 10.0 ± 0.2, E = 0.38 ± 0.02 V *vs.* SHE) media, respectively (orange points in Figure 1). The NaI-123 source was diluted into solutions with the same conditions as the ^{211}At samples. The eluents were freshly prepared by dilution of stock solutions. The samples of 10^{-5} M Br^-, 10^{-5} M $^{127}I^-$ and 10^{-5} M $S_2O_3^{2-}$ were prepared by dissolving the corresponding mass of NaBr, NaI–127 and $Na_2S_2O_3$ salts, respectively.

The HPIEC device used was a Dionex UltiMate3000 system consisting of a degasser, a DGP-3600 MB pump, a TCC-3200B column oven, and a diode array DAD-3000 detector. The stationary phase used was a Dionex AS20 anionic exchange column (0.2 cm diameter × 25 cm length), consisting of hydrophilic polymers grafted with quaternary alkanol ammonium, with a capacity of 77.5 µeq. It is pre-protected by a Dionex AG20 guard column (2 mm diameter × 50 mm length), with a capacity of 1.5 µeq. The device is coupled with an online γ-ray detector Raytest GabiStar, and is piloted by Gina Software. The experimental data are acquired and processed by Chromeleon 6.80 Chromatography Software. The retention time was taken at the maximum of the peak that belongs to the specific species (known or unknown) from the chromatogram.

All HPIEC measurements were performed under isocratic conditions at 25°C, with an eluent flow rate fixed at 350 µL·min^{-1}. Before each measurement, the column was equilibrated with eluent for at least 30 mins. $^{123}I^-$, $^{127}I^-$, Br^-, and $S_2O_3^{2-}$ were all detected online spectrophotometrically at 230 and 214 nm; ^{211}At and ^{123}I were detected by the γ-ray detector with the energy window set between 50 and 1630 keV.

The retention factor k is calculated as

$$k = \frac{t_\mathrm{r} - t_\mathrm{d}}{t_\mathrm{d}} \tag{10}$$

where t_r represents the retention time and t_d is the dead time of the device.

Electromobility measurements

The electromobility measurements are based on the electrophoresis phenomenon. The mobility of an ion at infinite dilution is a specific parameter for the ion, which depends on its charge/size ratio. In the present work, the reducing medium was composed of 10^{-4} M NaOH, 10^{-4} M DTT and 0.1 M NaCl (pH = 10.0 ± 0.2, E = –0.20 ± 0.02 V *vs.* SHE), and the oxidizing medium consisted of 10^{-4} M NaOH and 0.1 M $NaClO_4$ (pH = 10.0 ± 0.2, E = 0.40 ± 0.02 V *vs.* SHE) (orange points in Figure 1).

The device for measuring a radioactive ion mobility in free electrolytes was developed by Milanov *et al*.[40] A similar equipment was built in our laboratory in order to investigate the mobility of iodine and astatine ions. A detailed description can be found in the previous article.[15] Briefly, a horizontal glass tube is filled by the electrolyte solution. A high voltage is applied to the electrolyte solution, creating an electric field. The radioactive samples are injected into the electrolyte and the migration occurs in the horizontal glass tube. A gamma-ray detector continuously moves along the tube with a fixed speed, to monitor the distribution of radioactivity ions at different moments.

All the electromobility measurements were performed at 25°C (maintained by a water bath system). The voltage applied to the electromigration device was set at 450 ± 3 V. The injected activity of ^{123}I (E_γ = 159.97 keV, intensity 83.25%) was about 500 kBq and for ^{211}At (E_γ = 687 keV, intensity 0.245%) was about 1 MBq.

Liquid/liquid competition experiment

The principle of the liquid/liquid competition method is to track the distribution ratio of astatine between two immiscible liquid phases (*D*) as a function of influent physiochemical parameters (pH, Eh, *etc.*). A variation of *D* value caused by the change of experimental conditions must reveal an astatine speciation change in at least one of the two phases. In this work, all experiments were performed in air-conditioned laboratories (21 ± 3 °C). The aqueous phase was prepared with a pH buffer while adding redox agents to fix the potential. The pH buffer solutions for pH = 8 and 9 were prepared with 0.02 M PIPPS adjusted by 1 M NaOH. For pH = 11, the solution was directly prepared with 10^{-3} M NaOH. The organic phase was Diisopropyl ether (DIPE) pre-equilibrated with the corresponding pH buffer solution. For a series of experiments, the potential of samples was modified by changing the concentration of DTT from 10^{-3} M to 10^{-7} M, or by varying the $S_2O_8^{2-}/SO_4^{2-}$ redox couple concentration ratio while fixing $[Na_2S_2O_8] + [Na_2SO_4] = 10^{-3}$ M. The preparation allowed to obtain a series of aqueous solutions with the potential varied from –0.20 V to up to 0.35 V *vs.* SHE. NaOH was used to re-adjust the pH of samples if it was modified after the addition of the redox agents. Finally, ^{211}At stock solution recovered in the corresponding pH buffer solution was added in each sample. A 5 mL aliquot of organic and aqueous phases were brought into contact in Pyrex tubes. The tubes were shaken for 2 h to reach the equilibrium. Then, aliquots of the aqueous and organic phases were taken to measure the activity of each phase. All experiments were repeated at least twice under the same experimental conditions with different astatine sources.

The radioactivity in samples were measured using a Packard 2550 TR/AB Liquid Scintillation analyzer and the Ultima Gold LLT liquid scintillation cocktail. The quenching caused by different media was considered to determine the astatine activity (*A*) according to the following equation:

$$A = A_{\mathrm{mes}} \times (8.1063 \times 10^{-10} \times tSIE^3 - 1.7581 \times 10^{-6} \times tSIE^2 + 0.0012 \times tSIE + 0.7299) \quad (11)$$

with A_{mes} being the activity measured by a liquid scintillation counter and *tSIE* being the transformed Spectral Index of External standard defined by the apparatus for counting efficiency determination.

The distribution ratio of astatine is calculated by the following equation:

$$D = \frac{V_{\mathrm{aq}} \times A_{\mathrm{org}}}{V_{\mathrm{org}} \times A_{\mathrm{aq}}} \quad (12)$$

with A_{org}, A_{aq} the total activity in the organic and aqueous phases, respectively, and V_{org}, V_{aq} the volume of the organic and aqueous phases, respectively.

ASSOCIATED CONTENT

Supporting Information. The Supporting Information is available free of charge at xxxx.

Investigation of the interference of chemicals and astatine species, calculations of the apparent mobility of ions and supplementary figures and tables (PDF)

AUTHOR INFORMATION

Corresponding Author

*Julie.Champion@subatech.in2p3.fr

Present Addresses

†Laboratory of Radiochemistry, Paul Scherrer Institut, Forschungsstrasse 111, 5232, Villigen, PSI, Switzerland

Author Contributions

All the experiments were performed by L.L. The manuscript was written through contributions of all authors. All authors have given approval to the final version of the manuscript.

Notes

The authors declare no competing financial interest.

ACKNOWLEDGMENT

This work was supported in part by grants from the French National Agency for Research called Labex IRON (ANR-11-LABX-18-01). The authors acknowledge the GIP ARRONAX for the production of At-211.

REFERENCES

(1) Pourbaix, M. *Atlas of Electrochemical Equilibria in Aqueous Solutions*, 2nd ed.; Houston,Texas, 1974. https://doi.org/10.4028/www.scientific.net/msf.251-254.143.

(2) Marimuthu, V.; Dulac, I.; Kannoorpatti, K. Significance of Pourbaix Diagrams to Study the Corrosion Behaviour of Hardfacing Alloys Based on Chromium Carbides at 298 K (25 °C). *J. Bio- Tribo-Corrosion* **2016**, *2* (3), 17. https://doi.org/10.1007/s40735-016-0047-y.

(3) Ashby, M. F.; Jones, D. R. H. *Wet Corrosion of Materials*, 4th ed.; Elsevier Ltd., 2012.

(4) Yang, B.; Zeng, Z.; Wang, X.; Yin, X.; Chen, S. Pourbaix Diagrams to Decipher Precipitation Conditions of Si-Fe-Mn-Oxyhydroxides at the PACMANUS Hydrothermal Field. *Acta Oceanol. Sin.* **2014**, *33* (12), 58–66. https://doi.org/10.1007/s13131-014-0572-9.

(5) Corson, D. R.; MacKenzie, K. R.; Segrè, E. Artificially Radioactive Element 85. *Phys. Rev.* **1940**, *58* (8), 672–678. https://doi.org/10.1103/PhysRev.58.672.

(6) Kluetz, P. G.; Pierce, W.; Maher, V. E.; Zhang, H.; Tang, S.; Song, P.; Liu, Q.; Haber, M. T.; Leutzinger, E. E.; Al-Hakim, A.; Chen, W.; Palmby, T.; Alebachew, E.; Sridhara, R.; Ibrahim, A.; Justice, R.; Pazdur, R. Radium Ra 223 Dichloride Injection: U.S. Food and Drug Administration Drug Approval Summary. *Clin. Cancer Res.* **2014**, *20* (1), 9–14. https://doi.org/10.1158/1078-0432.CCR-13-2665.

(7) Zalutsky, M. R.; Reardon, D. A.; Akabani, G.; Coleman, R. E.; Friedman, A. H.; Friedman, H. S.; McLendon, R. E.; Wong, T. Z.; Bigner, D. D. Clinical Experience with -Particle Emitting 211At: Treatment of Recurrent Brain Tumor Patients with 211At-Labeled Chimeric Antitenascin Monoclonal Antibody 81C6. *J. Nucl. Med.* **2007**, *49* (1), 30–38. https://doi.org/10.2967/jnumed.107.046938.

(8) Andersson, H.; Cederkrantz, E.; Back, T.; Divgi, C.; Elgqvist, J.; Himmelman, J.; Horvath, G.; Jacobsson, L.; Jensen, H.; Lindegren, S.; Palm, S.; Hultborn, R. Intraperitoneal α-Particle Radioimmunotherapy of Ovarian Cancer Patients: Pharmacokinetics and Dosimetry of 211At-MX35 F(Ab')2—A Phase I Study. *J. Nucl. Med.* **2009**, *50* (7), 1153–1160. https://doi.org/10.2967/jnumed.109.062604.

(9) Wilbur, D. S. Enigmatic Astatine. *Nat. Chem.* **2013**, *5* (3), 246–246. https://doi.org/10.1038/nchem.1580.

(10) Guérard, F.; Maingueneau, C.; Liu, L.; Eychenne, R.; Gestin, J.-F.; Montavon, G.; Galland, N. Advances in the Chemistry of Astatine and Implications for the Development of Radiopharmaceuticals. *Acc. Chem. Res.* **2021**, *54* (16), 3264–3275.

https://doi.org/10.1021/acs.accounts.1c00327.

(11) Ruth, T. J.; Dombsky, M.; D'Auria, J. M.; Ward, T. E. *Radiochemistry of Astatine*; Office of scientific and technical information: U.S. Department of Energy, 1988. https://doi.org/10.2172/6748269.

(12) Berei, K.; Eberle, Siegfried H. Kirby, H. W.; Munzel, H.; Rossler, K.; Seidel, A.; Vasáros, L. *Gmelin Handbook of Inorganic Chemistry Astatine*, 8th ed.; Kugler, H. K., Keller, C., Eds.; Springer-Verlag Berlin Heidelberg, 1985. https://doi.org/10.1524/zpch.1969.66.1_3.165a.

(13) Cavallero, A.; Roessler, K. Chromatography at Fixed Redox Potential of Inorganic Forms of Astatine (211At). *Radiochim. Acta* **1989**, *47* (2–3), 113–117. https://doi.org/10.1524/ract.1989.47.23.113.

(14) Sabatié-Gogova, A.; Champion, J.; Huclier, S.; Michel, N.; Pottier, F.; Galland, N.; Asfari, Z.; Chérel, M.; Montavon, G. Characterization of At- Species in Simple and Biological Media by High Performance Anion Exchange Chromatography Coupled to Gamma Detector. *Anal. Chim. Acta* **2012**, *721*, 182–188. https://doi.org/10.1016/j.aca.2012.01.052.

(15) Guo, N.; Pottier, F.; Aupiais, J.; Alliot, C.; Montavon, G.; Champion, J. Evidence for the Heaviest Expected Halide Species in Aqueous Solution, At-, by Electromobility Measurements. *Inorg. Chem.* **2018**, *57* (9), 4926–4933. https://doi.org/10.1021/acs.inorgchem.7b03003.

(16) Liu, L.; Guo, N.; Champion, J.; Graton, J.; Montavon, G.; Galland, N.; Maurice, R. Towards a Stronger Halogen Bond Involving Astatine: Unexpected Adduct with Bu3PO Stabilized

by Hydrogen Bonding. *Chem. – A Eur. J.* **2020**, *26* (17), 3713–3717. https://doi.org/10.1002/chem.201905389.

(17) Guo, N.; Sergentu, D.-C.; Teze, D.; Champion, J.; Montavon, G.; Galland, N.; Maurice, R. The Heaviest Possible Ternary Trihalogen Species, IAtBr- , Evidenced in Aqueous Solution: An Experimental Performance Driven by Computations. *Angew. Chemie Int. Ed.* **2016**, *55* (49), 15369–15372. https://doi.org/10.1002/anie.201608746.

(18) Champion, J.; Alliot, C.; Renault, E.; Mokili, B. M.; Chérel, M.; Galland, N.; Montavon, G. Astatine Standard Redox Potentials and Speciation in Acidic Medium. *J. Phys. Chem. A* **2010**, *114* (1), 576–582. https://doi.org/10.1021/jp9077008.

(19) Champion, J.; Sabatié-Gogova, A.; Bassal, F.; Ayed, T.; Alliot, C.; Galland, N.; Montavon, G. Investigation of Astatine(III) Hydrolyzed Species: Experiments and Relativistic Calculations. *J. Phys. Chem. A* **2013**, *117* (9), 1983–1990. https://doi.org/10.1021/jp3099413.

(20) Champion, J.; Alliot, C.; Huclier, S.; Deniaud, D.; Asfari, Z.; Montavon, G. Determination of Stability Constants between Complexing Agents and At(I) and At(III) Species Present at Ultra-Trace Concentrations. *Inorganica Chim. Acta* **2009**, *362* (8), 2654–2661. https://doi.org/10.1016/j.ica.2008.12.005.

(21) Champion, J.; Seydou, M.; Sabatié-Gogova, A.; Renault, E.; Montavon, G.; Galland, N. Assessment of an Effective Quasirelativistic Methodology Designed to Study Astatine Chemistry in Aqueous Solution. *Phys. Chem. Chem. Phys.* **2011**, *13* (33), 14984. https://doi.org/10.1039/c1cp20512a.

(22) Liu, L.; Rahali, S.; Maurice, R.; Gomez Pech, C.; Montavon, G.; Le Questel, J. Y.; Graton, J.; Champion, J.; Galland, N. An Expanded Halogen Bonding Scale Using Astatine. *Chem. Sci.* **2021**, *12* (32), 10855–10861. https://doi.org/10.1039/d1sc02133h.

(23) Bassal, F.; Champion, J.; Pardoue, S.; Seydou, M.; Sabatié-Gogova, A.; Deniaud, D.; Questel, J. Y. Le; Montavon, G.; Galland, N. Questioning the Affinity of Electrophilic Astatine for Sulfur-Containing Compounds: Unexpected Bindings Revealed. *Inorg. Chem.* **2020**, *59* (19), 13923–13932. https://doi.org/10.1021/acs.inorgchem.0c01553.

(24) Guo, N.; Maurice, R.; Teze, D.; Graton, J.; Champion, J.; Montavon, G.; Galland, N. Experimental and Computational Evidence of Halogen Bonds Involving Astatine. *Nat. Chem.* **2018**, *10* (4), 428–434. https://doi.org/10.1038/s41557-018-0011-1.

(25) Sergentu, D.-C.; Teze, D.; Sabatié-Gogova, A.; Alliot, C.; Guo, N.; Bassal, F.; Silva, I. Da; Deniaud, D.; Maurice, R.; Champion, J.; Galland, N.; Montavon, G. Advances on the Determination of the Astatine Pourbaix Diagram: Predomination of AtO(OH)2- over At- in Basic Conditions. *Chem. - A Eur. J.* **2016**, *22* (9), 2964–2971. https://doi.org/10.1002/chem.201504403.

(26) Gjerde, D. T.; Schmuckler, G.; Fritz, J. S. Anion Chromatography with Low-Conductivity Eluents. II. *J. Chromatogr. A* **1980**, *187* (1), 35–45. https://doi.org/10.1016/S0021-9673(00)87871-1.

(27) Johnson, J.; Anderson, F.; Parkhurst, D. L. Database Thermo.Com.V8.R6.230, Rev 1.11. Lawrence Livermore National Laboratory: Livermore, California 2000.

(28) Réal, F.; Severo Pereira Gomes, A.; Guerrero Martínez, Y. O.; Ayed, T.; Galland, N.;

Masella, M.; Vallet, V. Structural, Dynamical, and Transport Properties of the Hydrated Halides: How Do At- Bulk Properties Compare with Those of the Other Halides, from F- to I-? *J. Chem. Phys.* **2016**, *144* (12). https://doi.org/10.1063/1.4944613.

(29) Appelman, E. H. The Oxidation States of Astatine in Aqueous Solution 1. *J. Am. Chem. Soc.* **1961**, *83* (4), 805–807. https://doi.org/10.1021/ja01465a014.

(30) Meyer, G.-J. Chromatographie Trägerfreier Anorganischer Formen von Jod-123 Und Astat-211 Und Ihre Verwendung Zur Halogenierung von Uracil and Desoxyuridin, University of Jülich, 1974.

(31) Tereshatov, E. E.; Burns, J. D.; Vonder Haar, A. L.; Schultz, S. J.; McIntosh, L. A.; Tabacaru, G. C.; McCann, L. A.; Avila, G.; Hannaman, A.; Lofton, K. N.; McCarthy, M. A.; Zhang, B.; Hall, M. B.; Yennello, S. J. Separation, Speciation, and Mechanism of Astatine and Bismuth Extraction from Nitric Acid into 1-Octanol and Methyl Anthranilate. *Sep. Purif. Technol.* **2022**, *282* (PB), 120088. https://doi.org/10.1016/j.seppur.2021.120088.

(32) Garaix, G.; Venault, L.; Costagliola, A.; Maurin, J.; Guigue, M.; Omnee, R.; Blain, G.; Vandenborre, J.; Fattahi, M.; Vigier, N.; Moisy, P. Alpha Radiolysis of Nitric Acid and Sodium Nitrate with 4He2+ Beam of 13.5 MeV Energy. *Radiat. Phys. Chem.* **2015**, *106* (2), 394–403. https://doi.org/10.1016/j.radphyschem.2014.08.008.

(33) Johnson, G. L.; Leininger, R. F.; Segrè, E. Chemical Properties of Astatine. I. *J. Chem. Phys.* **1949**, *17* (1), 1–10. https://doi.org/10.1063/1.1747034.

(34) Nishinaka, I.; Hashimoto, K.; Suzuki, H. Speciation of Astatine Reacted with Oxidizing and Reducing Reagents by Thin Layer Chromatography: Formation of Volatile Astatine. *J.*

Radioanal. Nucl. Chem. **2019**, *322* (3), 2003–2009. https://doi.org/10.1007/s10967-019-06900-3.

(35) Nishinaka, I.; Hashimoto, K.; Suzuki, H. Thin Layer Chromatography for Astatine and Iodine in Solutions Prepared by Dry Distillation. *J. Radioanal. Nucl. Chem.* **2018**, *318* (2), 897–905. https://doi.org/10.1007/s10967-018-6088-6.

(36) Rössler, K.; Tornau, W.; Stöcklin, G. Rapid Separation of Carrier-Free Inorganic and Organic Compounds of Radioiodine and Astatine by High-Pressure Liquid Chromatography. *J. Radioanal. Chem.* **1974**, *21* (1), 199–209. https://doi.org/10.1007/BF02520862.

(37) Dreyer, I.; Dreyer, R.; Chalkin, V. A. Kationen Des Astats in Wässrigen Lösungen: Darstellung Und Einige Eigenschaften. *J. Radiochem. Radioanal. Lett.* **1978**, *36* (6), 389–398.

(38) www.arronax-nantes.fr.

(39) Lindegren, S.; Bäck, T.; Jensen, H. J. Dry-Distillation of Astatine-211 from Irradiated Bismuth Targets: A Time-Saving Procedure with High Recovery Yields. *Appl. Radiat. Isot.* **2001**, *55* (2), 157–160. https://doi.org/10.1016/S0969-8043(01)00044-6.

(40) Milanov, M.; Doberenz, W.; Marinov, A.; Khalkin, V. A. Determination of Ion Mobilities of Radionuclides in a Free Electrolyte. Methods and Experimental Organization. *J. Radioanal. Nucl. Chem. Artic.* **1984**, *82* (1), 101–109. https://doi.org/10.1007/BF02227333.